Chaos, Solitons and Fractals 164 (2022) 112537

Contents lists available at ScienceDirect

Chaos, Solitons and Fractals

journal homepage: www.elsevier.com/locate/chaos

Computing using pulse collisions in lattices of excitable microlasers

L. Soun [a,*], K. Alfaro-Bittner [b], M.G. Clerc [c], S. Barbay [a]

[a] Université Paris-Saclay, CNRS, Centre de Nanosciences et de Nanotechnologies, 91120 Palaiseau, France
[b] Universidad Rey Juan Carlos, Calle Tulipán s/n, 28933 Móstoles, Madrid, Spain
[c] Departamento de Fśica and Millennium Institute for Research in Optics, FCFM, Universidad de Chile, Casilla 487-3, Santiago, Chile

ARTICLE INFO

Keywords:
Excitability
Pulse collision
Photonic computing
Logic gates
Coupled microlasers

ABSTRACT

Coupled excitable microlasers have been shown theoretically to sustain saltatory propagation of solitonic-like excitations and hold good promise for fabrication of advanced and integrated photonic processing circuits. By studying a model for evanescently coupled excitable microlaser lattices with integrated saturable absorber, we investigate how pulse interaction can lead to non trivial responses. In particular, we show in a three-port system that depending on the system parameters and geometry, two counter-propagating pulses from two input ports can collide and exit or not in a third port, thus giving rise to the not-linearly separable XOR response function and to universal logic gates.

1. Introduction

Excitability is a nonlinear generic phenomenon that results in an all-or-nothing response to an input perturbation. Neurons are endowed with this property [1,2], producing a calibrated pulse only if a certain excitation threshold is reached. Spatially extended excitable systems are well known to sustain the propagation of nonlinear waves [3–6]. Among the most well-known examples are excitable electrical waves in the cardiac tissue [7] and in the chicken retina [8], chemical excitable waves [9,10] in the spatially extended Belousov–Zhabotinsky (BZ) reaction and CO oxidation on platinum surfaces [11]. The nonlinear and collision properties of these waves have motivated the study of excitable logic in continuous [12–16] or discrete lattices [17,18]. However, the kinetic of chemical reactions is very slow and it is difficult to get integrated systems with a small footprint. Photonics technologies may circumvent these problems offering subnanosecond timescales for the material recovery times and tens of micrometer scale devices.

Excitable dynamics in optical systems has been studied and demonstrated since a long time [19,20]. Optical excitable waves have been predicted in broad area lasers [21] and studied experimentally in such a system [22] but a clear demonstration remains elusive. More recently it has been proposed to use lattices of semiconductor excitable microlasers [23]. These lattices are based on excitable micropillar semiconductor lasers [24,25], which are integrated devices with excitable response in the hundreds of picoseconds range. The propagation of excitations in chains of coupled excitable microlasers has been studied with a diffractive [26,27] and a diffusive optical coupling [28,29]. In a related study, similar waves have been studied in discretely coupled integrate-and-fire excitatory neurons [30].

When an excitable pulse is ignited in the lattice, a nonlinear soliton-like response can propagate in a saltatory manner between excitable nodes. The properties of this nonlinear propagating pulse are very interesting for optical computing and in the context of neuromorphic photonics, with the aim of developing computing optical devices inspired by the brain [25,31]. An architecture for an OR gate has been previously proposed [25], as well as a way to create an AND gate. It relies on the adjustment of the pumping of specific pillars in the lattice. Logic gates based on dissipative localized structures (cavity solitons) have been studied in [32], based on the local interaction between non-propagative optical coherent structures.

Here, we investigate suitable architectures to produce different logic gates allowing universal computation. These gates are based on the peculiar collision and propagation properties of the discrete excitable waves in micropillar laser lattices. As a matter of fact, we will show that a change in the coupling coefficient or pumping value in a lattice producing an OR gate can give rise to a XOR gate. We study the physics involved in this unexpected and non-trivial phenomenon. The XOR function is also interesting in a machine learning context as it implements a non separable problem and is often used as a test-bed for simple neural networks [33–35]. We demonstrate other logical gates, like the universal gates NAND and NOR, that can be cascaded to create any logical function.

2. Model

The architecture of a logical gate is described in Fig. 1. It is the association of N (even) excitable micropillar lasers [36]. The two inputs of

* Corresponding author.
E-mail address: lena.soun@c2n.upsaclay.fr (L. Soun).

https://doi.org/10.1016/j.chaos.2022.112537
Received 5 July 2022; Accepted 4 August 2022
Available online 6 September 2022

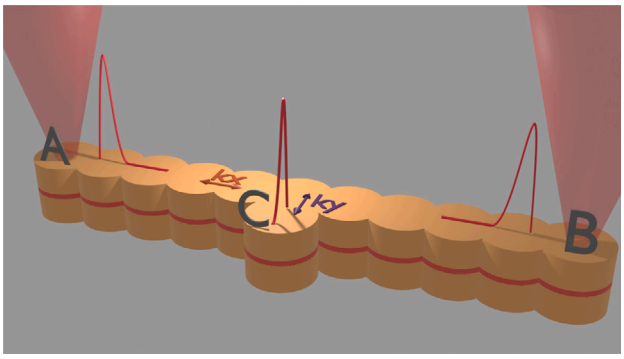

Fig. 1. Architecture of a logical gate: each micropillar has a few microns diameter, and is composed of a cavity formed by a top and a bottom Bragg mirror with an active medium (red) composed of gain and saturable absorber quantum wells (see [24] for details). Input pulses are sent at each extremities (A and B) of a lattice of coupled micropillars with a coupling factor κ_x. The output pillar (C) is coupled to the middle of the chain with a coupling factor κ_y. (For interpretation of the references to color in this figure legend, the reader is referred to the web version of this article.)

the logical gates are at both ends of the lattice and the input pulses sent to them are represented as red beams. The coupling factor κ_x between pillars is identical for all the chain, except for the output pillar connected to the micropillar at the middle of the chain with a coupling constant κ_y. The excitable micropillar laser emits perpendicularly to the surface.

The propagation of excitable pulses in this architecture can be simulated with a model of coupled ODEs [23]:

$$\dot{E}_j = \left[(1-i\alpha)G_j - (1-i\beta)Q_j - 1\right]E_j + \begin{cases} i\kappa_x E_{j-1} & \text{if } 1 < j \le N-1 \\ + \; i\kappa_x E_{j+1} & \text{if } 1 \le j < N-1 \\ + \; i\kappa_y E_N & \text{if } j = N/2 \\ + \; i\kappa_y E_{N/2} & \text{if } j = N, \end{cases} \tag{2.1a}$$

$$\dot{G}_j = b_1\left[\mu_1 - G_j(1+|E_j|^2)\right], \tag{2.1b}$$

$$\dot{Q}_j = b_2\left[\mu_2 - Q_j(1+s|E_j|^2)\right] \tag{2.1c}$$

with E_j, G_j, Q_j scaled adimensional variables: E_j representing the electric field envelope in the jth pillar, G_j the carrier density in the gain medium and Q_j the carrier density in the saturable absorber medium. The parameters are μ_1 the pump, μ_2 the linear absorption equal to 2, κ_x the coupling factor between the pillars of the chain along the long axis, κ_y the coupling factor of the output pillar (Nth pillar) with the middle of the chain, the gain and the carrier recombination rates b_1 and b_2 both equal to 0.002, the phase–amplitude coupling factors α and β respectively equal to 2 and 0, and s the saturation coefficient taken equal to 10. Time is rescaled to the electric-field decay time, which is on the order of a few picoseconds.

The initial conditions are given by:

$$\begin{aligned} E_j(t=0) &= \sqrt{I_{ss}} \times e^{i\phi_j} + \sqrt{I_{0j}} \\ G_j(t=0) &= \mu_1 \\ Q_j(t=0) &= \mu_2 \end{aligned} \tag{2.2}$$

with Iss = 10^{-5}, a small intensity due to spontaneous emission, ϕ_j a random phase and I_{0j} the input intensity, equal to zero except for the extremes pillars when there is an input ($A = 1$ for pillar 1 and $B = 1$ for pillar N − 1).

3. Propagation and collision

Each micropillar modeled with the previous parameters has an excitable response. It is therefore capable of emitting a pulse if the

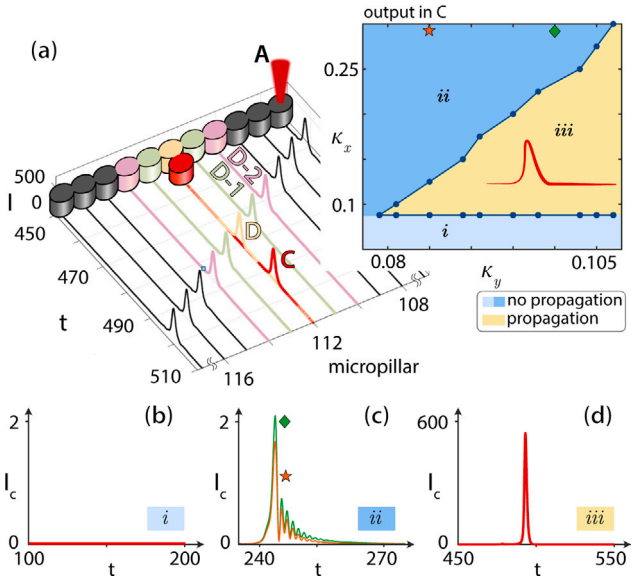

Fig. 2. Numerical simulations of Eqs. (2.1) when one of the edges is excited. (a) Spatiotemporal evolution of the pulse propagation. Pink, green, yellow, and red solid lines represents the response of $D-2$, $D-1$, D, and C cavities, respectively. Region in yellow (light blue) correspond the area where there is (there is no) an excitable response in C as a function of the coupling parameters (κ_x, κ_y). (b) Intensity profile (in C) as a function of time when $\kappa_x = 0.06, \kappa_y = 0.09$. (c) Intensity profiles measured in C when $\kappa_y = 0.09$ (orange solid line) and $\kappa_y = 0.095$ (green solid line) with $\kappa_x = 0.3$ in both cases. The red star (⋆) and the green diamond (⋄) indicates that these intensity profiles correspond to two points in the (κ_x, κ_y)-plane of the inset in panel (a). (c) Typical intensity profile of an excitable response with ($\kappa_x = 0.2$ and $\kappa_x = 0.115$). For all these simulations $\mu_1 = 2.75$, $\alpha = 2$, $\beta = 0$, $b_1 = b_2 = 0.002$, $\mu_2 = 2$, and $s = 10$. Initialization of the system: $I_{ss}, \phi_j = 0$, $I_{0A} = 10$ (coherent perturbation), and $j = 1, \ldots, 201$. (For interpretation of the references to color in this figure legend, the reader is referred to the web version of this article.)

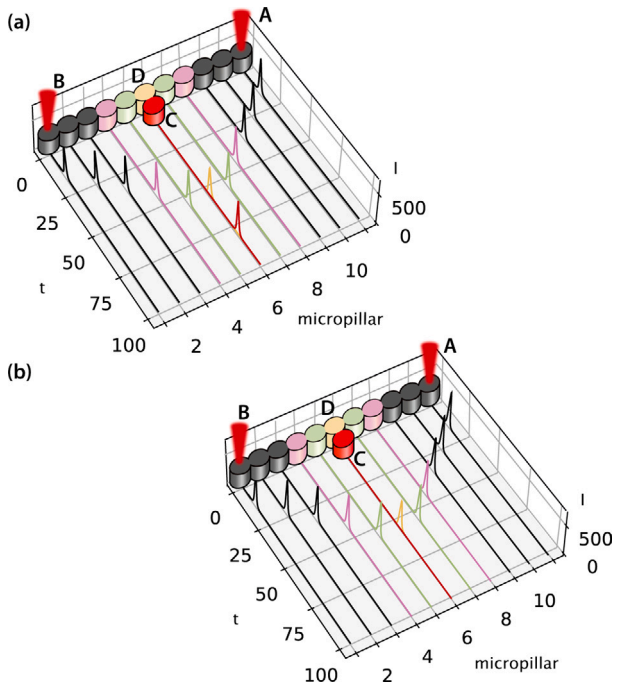

Fig. 3. Two different architectures, with input pillars A and B and output pillar C, and with parameters: $\mu_g = 2.8$, $\kappa_x = 0.1$ and $\kappa_y = 0.1$ in panel (a), $\kappa_y = 0.07$ in panel (b). The colors of the individual pillars correspond to the curves shown beside, where intensity versus time is plotted. Architecture represented in (a) corresponds to an OR gate, with a constructive pulse collision. Architecture represented in (b) behaves as a XOR gate, with inhibitory pulse collision. (For interpretation of the references to color in this figure legend, the reader is referred to the web version of this article.)

initial perturbation goes beyond a certain threshold, the excitable threshold, as shown theoretically in Refs. [37,38]. Excitability in such a micropillar has also been reported in experiment [24], including the demonstration of existence of refractory periods, spike latency [39], and temporal summation [40]. When the micropillars are coupled through the evanescent tail of their electric-field mode and one of the cavities is excited, a pulse propagating in a saltatory manner can be observed . The existence of a response in a chain of micropillars not only depends on the initial perturbation but also on the pump and on the coupling strength [25,26]. Indeed, in case of small coupling values, the propagation is triggered when the pump μ_1 also goes beyond a certain threshold that decreases almost linearly with coupling. Fig. 2 corresponds to numerical simulations of Eqs. (2.1) and shows how is the pulse propagation along the cavities when the first cavity (A) is perturbed coherently with light. Let us now consider, in the same figure, an output cavity (C) located in the middle of the main chain and colored in red. In particular, we use cavity C to study the properties of the propagation and interaction of pulses as a function of the coupling strength (between cavity C and the main chain). From the inset of Fig. 2(a), one can distinguish two main areas (light blue and yellow) depending on the coupling values. The yellow and light blue areas show the combination of (κ_x, κ_y) for which there is and there is no propagation in cavity C, respectively. The region in which there is no propagation is split into two zones, *i* and *ii*. The no propagation phenomenon has two different natures. In case of *i*, the pulse cannot propagate because for the pump value in the main chain $\mu_1 = 2.75$, the coherent perturbation is below the excitability threshold [26]. Indeed, the intensity profile in cavity C is zero, see Fig. 2(b). Contrarily to region *i*, in area *ii* the pump is not playing a crucial role because it is high enough for the couplings (κ_x and κ_y), i.e., there is always a pulse propagating over the main chain. In spite of the propagation, the evanescent tail of electric field coming from cavity (D) perturbs cavity (C) but is not capable to trigger an excitable response in it. In this situation, one measures in C an intensity whose maximum value is smaller [Fig. 2(c)] than the typical response [Fig. 2(d)]. Note that for a fixed value of κ_x, the output peak intensity measured in C increases as the coupling strength κ_y increases, as can be seen in the pulse profiles in Fig. 2(c). One then expect the evanescent coupling to overpass a certain threshold that depends on the coupling values between the main chain and the output micropillar.

The dynamics becomes richer when the main chain is simultaneously perturbed at the edges, i.e., at $j = 1$ (A) and $j = N - 1$ (B) (see Eqs. (2.2) for the initialization of the system). Depending on the collision between the pulses in the cavity, here called D, located at middle of the chain, and on the coupling value κ_y, the propagation in cavity C can be suppressed. Fig. 3 shows the spatiotemporal evolution of the pulses when they collide and interact "constructively" so that the cavity C has an excitable response (see panel (a) of the figure) or when the collision annihilates the excitable response in C [see panel (b)].

To understand the collision, we study the propagation throughout the main chain when the two cavities at the edges (A,B) are excited, see Fig. 4(a). For this purpose we have conducted simulations using the fourth-order Runge–Kutta algorithm and considered 201 micropillars to avoid any boundary or finite-size effect. In particular, we focus on the colored cavities next to C in Fig. 4(a). From Fig. 4(b) one observes that the intensity profile of cavities $D - 3$ (black line) and $D-2$ (pink line) are equal. The changes in the intensity profile become observable as the counterpropagative pulses reach cavity C. Indeed, the evanescent interaction makes the pulses smaller at cavity $D-1$ (green line) since, almost at the same time, cavity D is excited. Moreover, from the inset of the same figure, it can be observed how the right side of the pulses becomes monotonous as the propagation reaches the middle of the micropillar chain. Note that the collision of the evanescent tail of electric field at cavities $D-1$ makes the response in cavity D almost symmetric. The latter reveals that almost all the dynamic due to the collision is concentrated in cavity D.

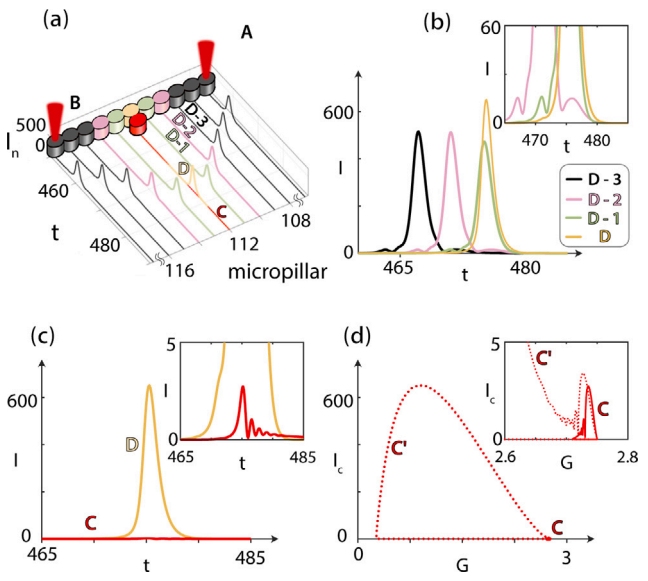

Fig. 4. Numerical simulations of Eqs. (2.1) when the edges of the main chain, i.e., A and B, are excited. (a) Spatiotemporal evolution of the pulse propagation. Black, pink, green, yellow, and red solid lines represents the response of $D-3$, $D-2$, $D-1$, D, and C cavities, respectively. (b) Intensity profile $D-3$, $D-2$, $D-1$, D as a function of time when $\kappa_x = 0.2$ and $\kappa_y = 0.114$. (c) Intensity profiles measured in D and C when $\kappa_x = 0.2$ and $\kappa_y = 0.114$. The inset corresponds to an amplification of the same figure. (d) $G-I$-phase space of the output cavity when $\kappa_y = 0.114$ (red dots, C) and $\kappa_y = 0.115$ (red solid line, C'). The inset corresponds to a zoom of the same figure. For all these simulations $\mu_1 = 2.75$, $\alpha = 2$, $\beta = 0$. Initialization of the system: $I_{ss}, \phi_j = 0$, $I_{0A} = 10$ (coherent perturbation), $\gamma = 0.002$, $\mu_2 = 2$, and $j = 1, \ldots, 201$. (For interpretation of the references to color in this figure legend, the reader is referred to the web version of this article.)

Table 1
The truth table for 8 logic gates: FALSE, logical conjunction AND, logical disjunction OR, exclusive disjunction XOR, logical NOR, logical NAND, logical biconditional XNOR and tautology TRUE.

(A, B)	FALSE	AND	OR	XOR
(1, 1)	0	1	1	0
(1, 0)	0	0	1	1
(0, 1)	0	0	1	1
(0, 0)	0	0	0	0
(A, B)	NOR	NAND	XNOR	TRUE
(1, 1)	0	0	1	1
(1, 0)	0	1	0	1
(0, 1)	0	1	0	1
(0, 0)	1	1	1	1

Let us remind that the pulse propagation occurs due to the perturbation made at one (or two) of the edges. This perturbation may generate an excitable response which may propagate to the next cavity by means of the evanescent tails of the electric field intensity. Note that this mechanism also holds for the interaction between the main chain and the output cavity (C). We then explore this evanescent interaction between cavity D and C when there is no output in C, as it is shown in Fig. 4(c). From the inset of this figure one can observe that at the same time the pulse in cavity D reaches its higher value, the evanescent tail of the electric field perturbs cavity C, however this perturbation is not enough to excite it. Fig. 4(d) illustrates the main features of this excitable system [37,38]. In particular, the red dots account for the situation in which there is an excitable response with $\kappa_x = 0.2$ and $\kappa_y = 0.115$ whereas the solid red line corresponds to the no propagation situation with $\kappa_x = 0.2$ and $\kappa_y = 0.114$. It can be observed from the inset of this figure that, for the same perturbation Eq. (2.2) with slightly different κ_y, the trajectory does a long (the pulse) or short excursion in the phase space before it returns to the stable state ($G_C = 2.75$, $I_C = 0$).

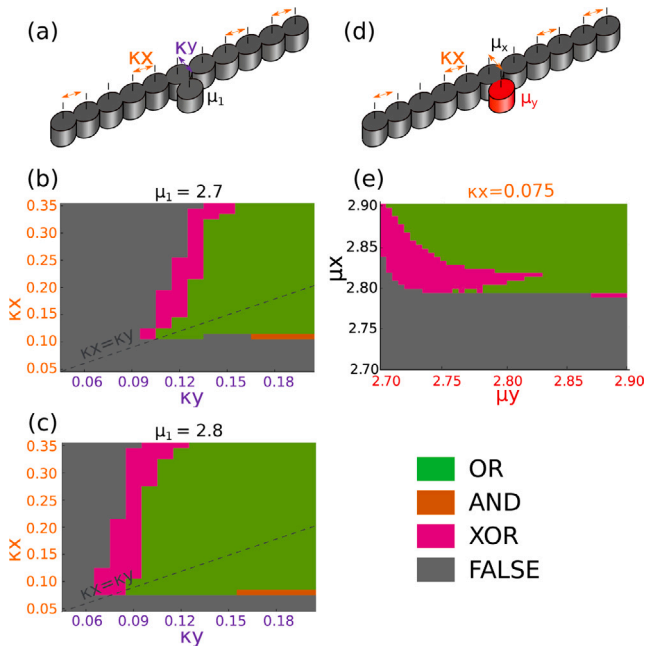

Fig. 5. Nature of the logical gate for different parameters: uniform pumping but different κ_x and κ_y for (b) and (c) [schematic in (a)] uniform coupling ($\kappa_x = 0.075$) but different pumping for cavity C [in (e), schematic in (d)]. (For interpretation of the references to color in this figure legend, the reader is referred to the web version of this article.)

Throughout this section, we have stated that in order to have pulse propagation along the entire micropillar lattice, the system must be initialized in such a way that the parameters (pump and coupling strength) go beyond of certain value. The latter holds independently of whether the propagation is triggered in one (A) or the two (A o B) micropillar edges. It is worth to note that the interaction and the subsequent collision of pulses make this system capable to compute Boolean functions as is shown in the next sections.

4. Logical gates

The architecture presented in Fig. 1 can be used to realize logical gates. This is based on the results demonstrated in the previous section, where a small change of the coupling factor κ_y can radically change the nature of the collision and subsequently of the signal in cavity C. Fig. 3 shows the evolution of the electric-field intensity following numerical integration of the model (Eqs. (2.1)) for two different gates, using this phenomenon. In the first one the coupling factors are all equal with $\kappa_x = 0.1$ and $\kappa_y = 0.1$. We can see in Fig. 3(a) that when two input perturbations (A = 1 and B = 1) are present, two counter-propagating pulses propagate in the chain from both sides, join in the middle micropillar, and reach the output pillar. In the same way, the gate produces a signal if only one perturbation is sent, and of course nothing when no perturbation are sent (results not shown). This is the behavior of an OR gate (see Table 1).

The second architecture, we describe in Fig. 3 uses the behavior described in Section 3. Thus, it differs from the first one only by the coupling factor κ_y for the output pillar, now at 0.07. That is, we increase the excitable threshold of the output micropillar. In practice, this is obtained by a larger center to center distance between the coupled pillars. In this case the propagation of two perturbations [cf. Fig. 3(b)] simultaneously arriving at the middle pillar do not produce an output pulse at the output pillar. However, a single perturbation sent at one of the ends of the lattice can elicit a response at the output pillar, that is can overcome the increase of the excitable threshold. This is the behavior of a XOR gate (see Table 1).

The study of the influence of different factors on the output state of the gate is presented in Fig. 5. The Fig. 5(b) and (c) show the gate resulting from the pulse collision in the (κ_x, κ_y) plane for different pumping values. We can see that the area of parameters for the OR behavior is dominant, and increases with the pump μ_1. Small zones for the AND gate appear at the limit with FALSE areas. These are limit cases when the coupling is so high that the propagation deviates from the pure saltatory propagation mode [26]. Most interestingly is the apparition of a large XOR zone where κ_y is smaller to κ_x. This XOR zone moves to smaller κ_y when the pumping increases [26]. Furthermore, we can obtain XOR gates by tuning the pumping of the output pillar alone, for a fixed coupling constant throughout the lattice as shown in Fig. 5(e). We see that we can also find a large zone of parameters for the XOR gate, without changing the architecture of the gate. This method offers a flexible way to tune the type of gate, since the coupling constant is fixed at the fabrication stage but the pump can be tuned during the experiment.

5. Universal gates

To complete the study, we explore the possibility to do universal gates, with which any logical operation is possible. We study in particular the NAND and NOR gates (see Table 1). These two logical operations bring another difficulty, as they require the generation of a signal without any perturbation (A = B = 0 and C = 1). We circumvent this difficulty by adding a pillar to the gate. This particular pillar is coupled to the middle of the chain and pumped over the self-pulsing threshold ($\mu_{th} = 3$), for a certain amount of time. Thus, this pillar produces pulses even with no input. Here, this pillar is pumped at ($\mu_{g2} = 3.15$), which results to a self-pulsing regime with a very long period, far higher than the simulation time. Thus, we see only one pulse produced by this pillar. The Fig. 6 presents the architecture of a NAND gate achieved with this solution. To achieve the NAND behavior (always '1' except when the two inputs are '1'), we keep the parameters used for the XOR gate, and we add the overpumped pillar. Then, if the two inputs are activated, the XOR behavior comes into play and annihilates the output signal in C [Fig. 6(a)].

A study of the influence of the parameters has also been done for this new architecture. It is shown in Fig. 7, where μ_1 and κ_y vary. We can see zones of NAND and NOR behavior at the frontier between the FALSE (always '0') and the TRUE (always '1'). We observe a linear dependence with the coupling κ_y and the pumping μ_1. This is due to the fact that these two parameters influence the propagation speed. Actually, the speed is a critical factor in the determination of the nature of the gate, because it relies on the synchronization of the pulses: for changing a NAND gate to a NOR gate (when $A = 1$ and $B = 0$, $C = 0$ instead of 1), we need to decrease a little the speed of the propagation in the main chain, so that when it arrives to the pillar D, it collides with the pulse of the overpumped pillar, giving no output. If we decrease even more the speed, the propagating pulse does not have time to reach the output before the end of the simulation, giving a FALSE. On the other hand, if we increase the speed, the XOR behavior is suppressed, so the gate always gives an output (TRUE). Indeed, the synchronization of the pulses relies also on the pump μ_{g2} because it determines the time when its pulse is produced. So, the map showed Fig. 7 will be slightly different with another μ_{g2}.

Consequently, this new architecture can produce all the logical gates described in Table 1.

6. Conclusion

In this paper, we propose architectures for realizing photonic logical gates, based on pulse collisions in microlaser lattices that can sustain solitonic-like excitation propagation. We have demonstrated that depending on the system parameters (coupling or pumping) we can get an OR gate or a XOR gate. Actually, there exists a sizeable range of

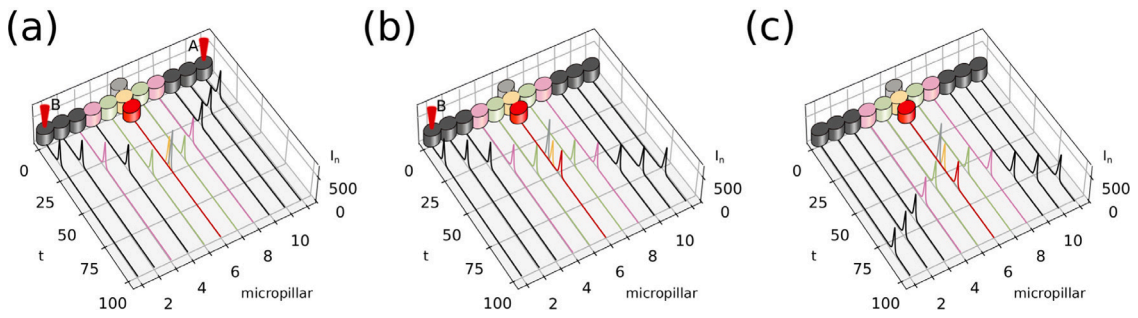

Fig. 6. NAND gate : (a) architecture with $\mu_g = 2.7$, $\kappa_x = 0.15$ and $\kappa_y = 0.12$. The overpumped pillar (in gray) is pumped at $\mu_{g2} = 3.15$. (b) Propagation in the gate when the two inputs are equal to 0. (c) With one input equal to 1. (d) The two input equal to 0. (For interpretation of the references to color in this figure legend, the reader is referred to the web version of this article.)

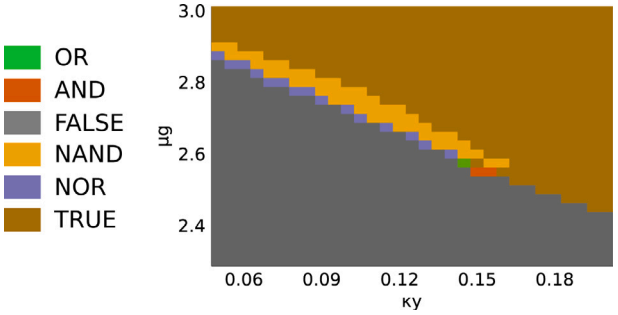

Fig. 7. Nature of the logical gate with an overpumped cavity at $\mu_{g2} = 3.15$, for different μ_1 and κ_y, with $\kappa_x = 0.2$. (For interpretation of the references to color in this figure legend, the reader is referred to the web version of this article.)

parameters where two counterpropagative pulses annihilate the signal in the output cavity, whereas only one input pulse does not. These architectures are flexible since one can tune either the pump or coupling strength to realize a specific gate. Moreover, we extended this study to the design of universal gates, which can produce any logical function and can be cascaded. Besides excitable logic, these demonstrations open interesting prospects for the experimental realization of more complex on-chip computing tasks taking advantage of the fast timescales and small system footprint, e.g. for spike time pattern recognition at high speed. On a more fundamental viewpoint, this system could also form an interesting photonic platform to study the propagation of nonlinear excitations in more complex lattice architectures or to investigate topological and non hermitian lattices [41].

Declaration of competing interest

The authors declare that they have no known competing financial interests or personal relationships that could have appeared to influence the work reported in this paper.

Data availability

Data will be made available on request.

Acknowledgments

L.S. and S.B. acknowledge funding from European Union Fun-COMP Project (#780848, Horizon 2020 Research and Innovation Program). MGC thanks for the financial support of ANID-Millennium Science Initiative Program ICN17-012 (MIRO) and FONDECYT Project No. 1210353.

References

[1] Izhikevich EM. Neural excitability, spiking and bursting. Int J Bifurcation Chaos 2000;10(06):1171–266.
[2] Izhikevich EM. Dynamical systems in neuroscience. MIT Press; 2007.
[3] Fitzhugh R. Computation of impulse initiation and saltatory conduction in a myelinated nerve fiber. Biophys J 1962;2(1):11–21.
[4] Elphick C, Meron E, Spiegel EA. Spatiotemporal complexity in traveling patterns. Phys Rev Lett 1988;61(5):496–9.
[5] Yamada H, Nozaki K. Interaction of pulses in dissipative systems: FitzHugh-Nagumo equations. Progr Theoret Phys 1990;84(5):801–9.
[6] Cross MC, Hohenberg PC. Pattern formation outside of equilibrium. Rev Modern Phys 1993;65(3):851–1112.
[7] Adelman W. Biophysics and physiology of excitable membranes. Van Nostrand; 1971.
[8] Gorelova NA, Bureš J. Spiral waves of spreading depression in the isolated chicken retina. J Neurobiol 1983;14(5):353–63.
[9] Zaikin AN, Zhabotinsky AM. Concentration wave propagation in two-dimensional liquid-phase self-oscillating system. Nature 1970;225(5232):535–7.
[10] Murray JD. Mathematical biology. Springer New York; 2002.
[11] Jakubith S, Rotermund HH, Engel W, von Oertzen A, Ertl G. Spatiotemporal concentration patterns in a surface reaction: Propagating and standing waves, rotating spirals, and turbulence. Phys Rev Lett 1990;65(24):3013–6.
[12] Hjelmfelt A, Ross J. Implementation of logic functions and computations by chemical kinetics. Phys D 1995;84(1–2):180–93.
[13] Adamatzky A, De Lacy Costello B. Experimental logical gates in a reaction-diffusion medium: The XOR gate and beyond. Phys Rev E 2002;66(4):046112.
[14] Adamatzky A. Collision-based computing in Belousov–Zhabotinsky medium. Chaos Solitons Fractals 2004;21(5):1259–64.
[15] De Lacy Costello B, Adamatzky A. Experimental implementation of collision-based gates in Belousov–Zhabotinsky medium. Chaos Solitons Fractals 2005;25(3):535–44.
[16] Motoike I, Adamatzky A. Three-valued logic gates in reaction–diffusion excitable media. Chaos Solitons Fractals 2005;24(1):107–14.
[17] Adamatzky A. Universal dynamical computation in multidimensional excitable lattices. Int J Theor Phys 1998;37(12):3069–108.
[18] Holley J, Jahan I, De Lacy Costello B, Bull L, Adamatzky A. Logical and arithmetic circuits in Belousov-Zhabotinsky encapsulated disks. Phys Rev E 2011;84(5):056110.
[19] Plaza F, Velarde MG, Arecchi FT, Boccaletti S, Ciofini M, Meucci R. Excitability following an avalanche-collapse process. Europhys Lett 1997;38(2):85–90.
[20] Giudici M, Green C, Giacomelli G, Nespolo U, Tredicce JR. Andronov bifurcation and excitability in semiconductor lasers with optical feedback. Phys Rev E 1997;55(6):6414–8.
[21] Coullet P, Daboussy D, Tredicce JR. Optical excitable waves. Phys Rev E 1998;58(5):5347–50.
[22] Marino F, Balle S. Excitable optical waves in semiconductor microcavities. Phys Rev Lett 2005;94(9).
[23] Barbay S, Sagnes I, Kuszelewicz R, Yacomotti AM. Localized states and excitability in a monolithic VCSEL with saturable absorber. In: 2011 fifth Rio de la plata workshop on laser dynamics and nonlinear photonics. IEEE; 2011, p. 1–4.
[24] Selmi F, Braive R, Beaudoin G, Sagnes I, Kuszelewicz R, Barbay S. Relative refractory period in an excitable semiconductor laser. Phys Rev Lett 2014;112:183902, & Synposis in Physics, Semiconductors Laser Get Nervy.
[25] Pammi VA, Alfaro-Bittner K, Clerc MG, Barbay S. Photonic computing with single and coupled spiking micropillar lasers. IEEE J Sel Top Quantum Electron 2020;26(1):1–7.
[26] Alfaro-Bittner K, Barbay S, Clerc MG. Pulse propagation in a 1D array of excitable semiconductor lasers. Chaos 2020;30(8):083136.

[27] Lamperti M, Perego AM. Collective dynamics of evanescently coupled excitable lasers with saturable absorber. Eur Phys J B 2019;92(6).
[28] Perego AM, Lamperti M. Collective excitability, synchronization, and array-enhanced coherence resonance in a population of lasers with a saturable absorber. Phys Rev A 2016;94(3):033839.
[29] Lamperti M, Perego AM. Disorder-induced localization of excitability in an array of coupled lasers. Phys Rev A 2017;96(4):041803.
[30] Badel L, Tonnelier A. Pulse propagation in discrete excitatory networks of integrate-and-fire neurons. Phys Rev E 2004;70(1).
[31] Nahmias MA, Shastri BJ, Tait AN, Prucnal PR. A leaky integrate-and-fire laser neuron for ultrafast cognitive computing. IEEE J Sel Top Quantum Electron 2013;19(5):1–12.
[32] Jacobo A, Gomila D, Matías MA, Colet P. Logical operations with localized structures. New J Phys 2012;14(1):013040.
[33] Brouwer R. Implementation of the exclusive-or function in a hopfield style recurrent network. Neural Process Lett 1997;5(1):1–7.
[34] Cyr A, Thériault F, Chartier S. Revisiting the XOR problem: a neurorobotic implementation. Neural Comput Appl 2019;32(14):9965–73.
[35] Lin C-E, Lu Y-H, Lin Y-T, Chen Y-F, Sun C-P, Chen C-C. All optical XOR logic gate formed by unsupervised optical neuron networks. Neurocomputing 2021;460:205–10.
[36] Elsass T, Gauthron K, Beaudoin G, Sagnes I, Kuszelewicz R, Barbay S. Control of cavity solitons and dynamical states in a monolithic vertical cavity laser with saturable absorber. Eur Phys J D 2010;59(1):91–6.
[37] Dubbeldam JLA, Krauskopf B, Lenstra D. Excitability and coherence resonance in lasers with saturable absorber. Phys Rev E 1999;60(6):6580–8.
[38] Dubbeldam JLA, Krauskopf B. Self-pulsations of lasers with saturable absorber : dynamics and bifurcations. Opt Commun 1999;159:325.
[39] Selmi F, Braive R, Beaudoin G, Sagnes I, Kuszelewicz R, Erneux T, Barbay S. Spike latency and response properties of an excitable micropillar laser. Phys Rev E 2016;94:042219.
[40] Selmi F, Braive R, Beaudoin G, Sagnes I, Kuszelewicz R, Barbay S. Temporal summation in a neuromimetic micropillar laser. Opt Lett 2015;40(23):5690–3.
[41] Ozawa T, Price HM, Amo A, Goldman N, Hafezi M, Lu L, Rechtsman MC, Schuster D, Simon J, Zilberberg O, Carusotto I. Topological photonics. Rev Modern Phys 2019;91(1):015006.